Design of the Optimum Pilot Pattern for Channel Estimation in OFDM Systems

Ji-Woong Choi and Yong-Hwan Lee
School of Electrical Engineering and INMC, Seoul National University
Kwanak P. O. Box 34, Seoul, 151-600, Korea
e-mail: jwch@fruit.snu.ac.kr, ylee@snu.ac.kr

Abstract - **The performance of channel estimation in OFDM systems significantly depends on the pilot signal, which is usually scattered in the time and frequency domains. For a given pilot density, we analytically design the optimum pilot pattern that minimizes the mean square error of the channel estimate obtained with the use of general interpolators. The analytic results are verified by computer simulation.**

I. INTRODUCTION

Orthogonal frequency division multiplexing (OFDM) systems often employ coherent detection that requires accurate information on the channel impulse response (CIR). The CIR can be estimated using predetermined pilot symbols in real time. In the OFDM system, the pilot symbols are scattered in the time and frequency domain to track time-variant and frequency selective channel characteristics. The CIR for coherent detection of data signal can be obtained by interpolating the CIR estimated using the pilot symbols.

The optimum interpolation can be performed using a two-dimensional (2-D) Wiener interpolator with infinite tap size. The mean square error (MSE) of the Wiener channel estimate only depends upon the pilot density, not the pilot pattern [1]. However, it may not be practical to use such a Wiener scheme because of large implementation complexity. As a result, a simple interpolator such as linear, Lagrange or Spline interpolation scheme is often employed in practice [2,3]. When these interpolators are employed, the performance of channel estimation is affected by the pilot pattern (i.e., the shape and spacing) as well as the pilot density [4-7]. For example, when the channel is fast time-variant with a small multipath delay spread, it would be advantageous to insert more pilot symbols in the time domain than in the frequency domain, and vice versa.

Most of previous researches on the design of pilot signal for channel estimation in mobile OFDM systems have been obtained based on the computer simulation results [4-7]. It is desirable to design the pilot pattern in an analytic manner without the need of exhaustive computer simulation. In this paper, for a given pilot density, we analytically derive the shape and spacing of the optimum pilot pattern by minimizing the MSE of the estimated CIR with the use of a conventional interpolator.

Following Introduction, the system and channel model are described in Section II. In Section III, the optimum pilot pattern is derived and its performance is verified by computer simulation. Finally, concluding remarks are summarized in Section IV.

II. SYSTEM MODEL

In the OFDM transmitter, K data symbols at the n-th symbol time, $\{X[n,k]\}$, k=0, 1, 2,…, K-1, are converted into a time domain signal using the inverse fast Fourier transform (FFT). A cyclic prefix (CP) is inserted to preserve the orthogonality between the subcarriers and to eliminate the interference between the adjacent OFDM symbols.

We consider the transmission of OFDM signal over a wireless channel whose impulse response is represented as

$$h(t,\tau)=\sum_{l=0}^{L-1}h_l(t)\delta(\tau-\tau_l) \tag{1.}$$

where L is the number of multipaths, $\delta(\cdot)$ is Kronecker delta function, τ_l and $h_l(t)$ denote the delay and complex-valued CIR at time t of the l-th path, respectively. We assume that $h_l(t)$ is statistically independent for each path and has the same normalized correlation function $r_t(\triangle t)$ for all l. Then, the time-domain correlation function of the l-th path CIR can be represented as

$$r_l(\triangle t)=E\{h_l(t+\triangle t)h_l^*(t)\}=\sigma_l^2 r_t(\triangle t) \tag{2.}$$

where $E\{X\}$ denotes the expectation of X, the superscript * denotes complex conjugate and σ_l^2 denotes the average power of the l-th path. The frequency response of the CIR at time t can be

represented as

$$H(t,f)=\int_{-\infty}^{\infty} h(t,\tau)\,\mathrm{e}^{-j2\pi f\tau}d\tau. \tag{3.}$$

Assuming the normalized average path power (i.e., $\sum_{l=0}^{L-1}\sigma_l^2=1$), the correlation function of the frequency response can be represented as

$$\begin{aligned} r_H(\triangle t,\triangle f) &= E\{H(t+\triangle t, f+\triangle f)H^*(t,f)\} \\ &= r_t(\triangle t)r_f(\triangle f) \end{aligned} \tag{4.}$$

where $r_f(\triangle f)=\sum_{l=0}^{L-1}\sigma_l^2\,\mathrm{e}^{-j2\pi\triangle f\tau_l}$. In an OFDM symbol with symbol time T_s and subcarrier spacing $\triangle f$, the correlation function can be represented as

$$r_H[n,k]=r_t[n]r_f[k] \tag{5.}$$

where $r_t[n]=r_t(nT_s)$ and $r_f[k]=r_f(k\triangle f)$. The corresponding spectrum of the channel correlation can be as

$$\begin{aligned} S_H(w_1,w_2) &= \sum_{n=-\infty}^{\infty}\sum_{k=-\infty}^{\infty} r_H[n,k]e^{-j(w_1n+w_2k)} \\ &= \sum_{n=-\infty}^{\infty} r_t[n]e^{-jw_1n}\cdot\sum_{k=-\infty}^{\infty} r_f[k]e^{-jw_2k} \\ &= S_{H_1}(w_1)S_{H_2}(w_2) \end{aligned} \tag{6.}$$

where $S_{H_1}(w_1)$ and $S_{H_2}(w_2)$ are the Fourier transform (FT) of $r_t[n]$ and $r_f[k]$, respectively.

In the receiver, the CP is removed before the FFT process. Assuming ideal synchronization at the receiver, the received symbol of the *k*-th subcarrier at the *n*-th symbol time can be represented by

$$Y[n,k]=X[n,k]H[n,k]+Z[n,k] \tag{7.}$$

where $H[n,k]$ is the frequency response of the channel at the *k*-th subcarrier and the *n*-th symbol time, and $Z[n,k]$ is the background noise plus interference term, which can be approximated as zero mean additive white Gaussian noise (AWGN) with variance σ_Z^2.

III. OPTIMUM PILOT PATTERN

We consider pilot patterns having a regular structure for practical implementation. Fig. 1 depicts various pilot patterns on the 2-D time-frequency grid for OFDM systems. A regularly arranged pilot symbol can be represented using two basis vectors $\nu_1=[x_1,y_1]^T$ and $\nu_2=[x_2,y_2]^T$ as shown in Fig. 2, where the vectors are represented in the Cartesian coordinate: the time axis by abscissa and the frequency axis by ordinate. Then, all the pilot patterns with a regular structure can be represented by these

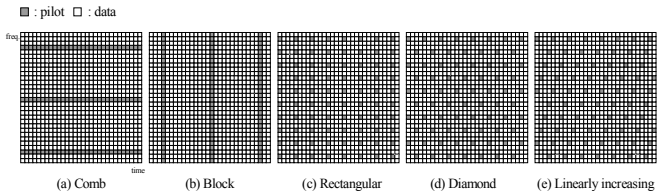

Fig. 1. Pilot arrangement on a 2-D grid.

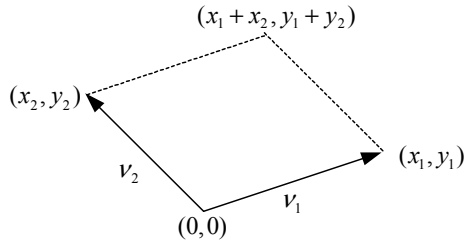

Fig. 2. Pilot pattern in the Cartesian coordinate.

two basis vectors. Since the pilot density D is inversely proportional to the pilot spacing, it can be defined as the inverse of the area of parallelogram formed by ν_1 and ν_2, i.e.,

$$D\equiv\left|\det(\boldsymbol{V})\right|^{-1}=\left|x_1y_2-x_2y_1\right|^{-1} \tag{8.}$$

where $\boldsymbol{V}=[\nu_1\ \nu_2]$ is a (2×2) matrix representing the pilot pattern. Although x_1, x_2, y_1 and y_2 can be any value, we assume $y_1=0$ without the loss of generality since any parallelogram can be made to $y_1=0$ by rotating the pattern.

The CIR corresponding to the pilot symbol is first estimated as

$$\tilde{H}[n_p,k_p]=Y[n_p,k_p]/X[n_p,k_p]=H[n_p,k_p]+\tilde{Z}[n_p,k_p] \tag{9.}$$

where n_p and k_p denote the symbol and the subcarrier index of pilot symbol, respectively, and $\tilde{Z}[n_p,k_p]$ denotes the noise term. Assuming $X[n_p,k_p]=1$, $\tilde{Z}[n_p,k_p]$ can be assumed zero mean AWGN with variance σ_Z^2. The CIR can be obtained by interpolating the CIR estimated from the pilot symbols as

$$\hat{H}[n,k]=\sum_{p=-\infty}^{\infty}\sum_{q=-\infty}^{\infty}\tilde{H}_s[n+p,k+q]w[p,q] \tag{10.}$$

where $\tilde{H}_s[n,k]$ is equal to $\tilde{H}[n,k]$ for the pilot symbol and zero, otherwise, and $w[p,q]$ denotes the coefficient of the interpolator. We consider the use of two 1-D interpolators for 2-D interpolation, i.e., one in the time domain and the other one in the frequency domain, to reduce the computational complexity without noticeable performance degradation [8].

When there is no interference, perfect CIR can be represented using an ideal interpolator as

$$H[n,k]=\sum_{p=-\infty}^{\infty}\sum_{q=-\infty}^{\infty}H_s[n+p,k+q]w_{id}[p,q] \qquad (11.)$$

where $H_s[n,k]$ is equal to $H[n,k]$ at the pilot symbol and zero, otherwise, and $w_{id}[p,q]$ is the coefficient of an ideal non-causal 2-D interpolator represented as [9]

$$w_{id}[p,q]=\frac{\sin(\pi p/x_1)\sin(\pi q/y_2)}{(\pi p/x_1)(\pi q/y_2)}. \qquad (12.)$$

Then, (10) can be rewritten as

$$\begin{aligned}\hat{H}[n,k]&=\sum_{p=-\infty}^{\infty}\sum_{q=-\infty}^{\infty}\left(H_s[n+p,k+q]+Z_s[n+p,k+q]\right)w[p,q]\\&+\left(H[n,k]-\sum_{p=-\infty}^{\infty}\sum_{q=-\infty}^{\infty}H_s[n+p,k+q]w_{id}[p,q]\right)\\&=H[n,k]+\sum_{p=-\infty}^{\infty}\sum_{q=-\infty}^{\infty}H_s[n+p,k+q]\left(w[p,q]-w_{id}[p,q]\right)\\&+\sum_{p=-\infty}^{\infty}\sum_{q=-\infty}^{\infty}Z_s[n+p,k+q]w[p,q]\end{aligned} \qquad (13.)$$

where $Z_s[n,k]$ is the additive noise term equal to $\tilde{Z}[n,k]$ at the pilot symbol and zero, otherwise. Note that the first term of (13) is the desired CIR, the second term is the self-distorted noise due to the use of a non-ideal interpolator and the third term is the interference due to the background noise plus interference.

The MSE of the CIR estimate can be represented as

$$\begin{aligned}\sigma_e^2&=E\left\{|\hat{H}[n,k]-H[n,k]|^2\right\}\\&=\frac{1}{(2\pi)^2}\int_{-\pi}^{\pi}\int_{-\pi}^{\pi}S_{H_s}(w_1,w_2)|W_e(w_1,w_2)|^2dw_1\,dw_2\\&+\frac{\sigma_Z^2 D}{(2\pi)^2}\int_{-\pi}^{\pi}\int_{-\pi}^{\pi}|W(w_1,w_2)|^2dw_1\,dw_2\\&=\sigma_S^2+\sigma_I^2\end{aligned} \qquad (14.)$$

where σ_S^2 and σ_I^2 are respectively the MSE due to the self-distortion and interference, and $S_{H_s}(w_1,w_2)$ is the sampled $S_H(w_1,w_2)$ [10],

$$S_{H_s}(w_1,w_2)=\frac{1}{(x_1y_2)^2}\sum_{n=0}^{x_1-1}\sum_{k=0}^{y_2-1}S_H\left(w_1-\frac{2\pi}{x_1}n,w_2-\frac{2\pi}{y_2}k-\frac{2\pi x_2}{x_1y_2}n\right). \qquad (15.)$$

Defining the interpolation error coefficient due to non-ideal interpolation by

$$w_e[p,q]=w[p,q]-w_{id}[p,q], \qquad (16.)$$

the 2-D FT of $w_e[p,q]$ can be represented as

$$W_e(w_1,w_2)=\begin{cases}W(w_1,w_2)-x_1y_2, & |w_1|\le\pi/x_1 \text{ and } |w_2|\le\pi/y_2\\ W(w_1,w_2), & \text{otherwise}\end{cases} \qquad (17.)$$

where $W(w_1,w_2)$ is the 2-D FT of $w[p,q]$. For example, $W(w_1,w_2)$ of a linear interpolator can be represented as [9]

$$W(w_1,w_2)=\frac{1}{x_1y_2}\left[\frac{\sin(w_1x_1/2)}{\sin(w_1/2)}\frac{\sin(w_2y_2/2)}{\sin(w_2/2)}\right]^2. \qquad (18.)$$

Since σ_I^2 is independent of the pilot shape, the optimum pilot pattern should be designed to minimize σ_S^2 for a given interpolator. For example, Fig. 3 depicts $S_{H_s}(w_1,w_2)$ and $|W_e(w_1,w_2)|^2$ when a linear interpolator is employed, where f_d and $\tau_{\max}$

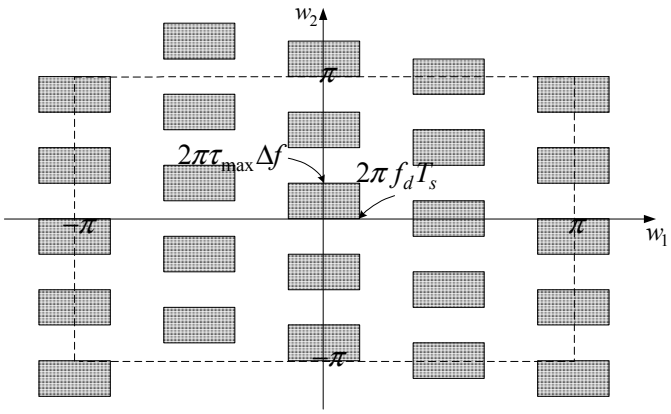

(a) $S_{H_s}(w_1,w_2)$

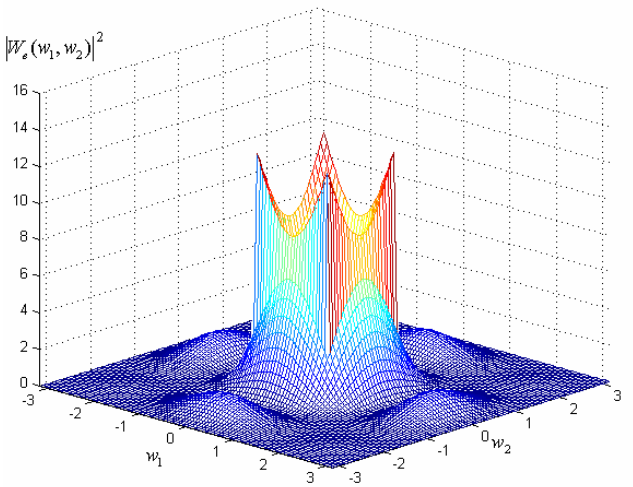

(b) $|W_e(w_1,w_2)|^2$ of linear interpolator

Fig. 3. 2-D spectrum of the channel correlation and interpolation error when $x_1=y_2=4$ and $x_2=1$.

denote the maximum Doppler frequency and maximum delay of the channel, respectively. For given x_1 and y_2, σ_S^2 depends on x_2 due to the MSE difference outside the passband, i.e., $w_1 \notin [-\pi/x_1 \ \pi/x_1]$ and $w_2 \notin [-\pi/y_2 \ \pi/y_2]$. Using the symmetrical property, it can easily be shown that σ_S^2 is minimized when $x_2 = x_1/2$, (i.e., a diamond shape) as the simulation results in [5]. However, the variation of σ_S^2 due to x_2 is marginal since the MSE resulted from the spectrum outside the passband is usually much smaller than that in the passband as seen in Fig. 3 (b).

Neglecting the MSE outside the passband and using a Taylor series approximation of $|W_e(w_1, w_2)|^2$, σ_S^2 can be approximated as

$$\begin{aligned}\sigma_S^2 &\approx \frac{1}{(2\pi)^2}\int_{-\pi/y_2}^{\pi/y_2}\int_{-\pi/x_1}^{\pi/x_1} S_{H_s}(w_1,w_2)\left(c_{IF,0}w_1^2w_2^2 + c_{IF,1}w_1^4 + c_{IF,2}w_2^4\right)dw_1\,dw_2 \\ &= \frac{1}{(x_1y_2)^2(2\pi)^2}\int_{-\pi}^{\pi}\int_{-\pi}^{\pi} S_{H_1}(w_1)S_{H_2}(w_2)\left(c_{IF,0}w_1^2w_2^2 + c_{IF,1}w_1^4 + c_{IF,2}w_2^4\right)dw_1\,dw_2 \\ &= \frac{1}{(x_1y_2)^2}\left(c_{IF,0}\overline{w}_1^{(2)}\overline{w}_2^{(2)} + c_{IF,1}\overline{w}_1^{(4)} + c_{IF,2}\overline{w}_2^{(4)}\right)\end{aligned} \tag{19.}$$

where $\overline{w}_1^{(n)}$ and $\overline{w}_2^{(n)}$ are respectively the *n*-th order moment of the Doppler spectrum and power delay profile represented as

$$\overline{w}_1^{(n)} = \frac{1}{2\pi}\int_{-\pi}^{\pi} w_1^n S_{H_1}(w_1)dw_1 \qquad \overline{w}_2^{(n)} = \frac{1}{2\pi}\int_{-\pi}^{\pi} w_2^n S_{H_2}(w_2)dw_2 \tag{20.}$$

and $c_{IF,0}$, $c_{IF,1}$ and $c_{IF,2}$ are the coefficients of the approximated polynomial of $|W_e(w_1, w_2)|^2$. Note that $\overline{w}_1^{(n)}$ and $\overline{w}_2^{(n)}$ depend on the correlation function of the channel, while $c_{IF,0}$, $c_{IF,1}$ and $c_{IF,2}$ depend on the interpolator.

Assume that x_1 and y_2 are continuous parameters for ease of analytic design. The optimum spacing $\hat{x}_1$ and $\hat{y}_2$ can uniquely be determined by solving

$$\left.\frac{\partial\sigma_S^2}{\partial x_1}\right|_{x_1=\hat{x}_1} = 0 \ \text{ and } \ \left.\frac{\partial\sigma_S^2}{\partial y_2}\right|_{y_2=\hat{y}_2} = 0. \tag{21.}$$

The spacing of the optimum pilot symbol should be determined considering the interpolator type, the moment of the Doppler spectrum and the power-delay profile of the channel. As an example, when a linear interpolator is employed for channel estimation, we consider the spacing of the optimum pilot pattern. In this case, $c_{IF,0}$, $c_{IF,1}$ and $c_{IF,2}$ can be represented as a function of x_1 and y_2 assuming $x_1^2, y_2^2 \gg 1$ as

$$\begin{aligned} c_{IF,0} &= (x_1^2-1)(y_2^2-1)/(72D^2) \\ &\approx x_1^2y_2^2/(72D^2) \\ c_{IF,1} &= (x_1^2-1)^2/(144D^2) \\ &\approx x_1^4/(144D^2) \\ c_{IF,1} &= (y_2^2-1)^2/(144D^2) \\ &\approx y_2^4/(144D^2). \end{aligned} \tag{22.}$$

Thus, σ_S^2 can be approximated as

$$\begin{aligned}\sigma_S^2 &\approx \frac{2D^{-2}\overline{w}_1^{(2)}\overline{w}_2^{(2)} + \overline{w}_1^{(4)}x_1^4 + \overline{w}_2^{(4)}y_2^4}{144} \\ &\geq \frac{\overline{w}_1^{(2)}\overline{w}_2^{(2)} + \sqrt{\overline{w}_1^{(4)}\overline{w}_2^{(4)}}}{72D^2}\end{aligned} \tag{23.}$$

where the equality holds when

$$\overline{w}_1^{(4)}x_1^4 = \overline{w}_2^{(4)}y_2^4. \tag{24.}$$

Using (24) and $D^{-1} = x_1y_2$, the optimum spacing $\hat{x}_1$ and $\hat{y}_2$ are determined as

$$\hat{x}_1 = D^{-0.5}\left(\frac{\overline{w}_2^{(4)}}{\overline{w}_1^{(4)}}\right)^{1/8} \qquad \hat{y}_2 = D^{-0.5}\left(\frac{\overline{w}_2^{(4)}}{\overline{w}_1^{(4)}}\right)^{-1/8}. \tag{25.}$$

For a given pilot density, the pilot symbol should be inserted considering the fourth-order moment of the Doppler spectrum and power-delay profile of the channel. When the mobility decreases (i.e., $\overline{w}_1^{(4)}$ decreases), it is required to increase $\hat{x}_1$ and decrease $\hat{y}_2$. When $\overline{w}_1^{(4)}$ goes to zero, $\hat{x}_1$ goes to infinite while $\hat{y}_2$ goes to zero, resulting a block type pilot pattern as in Fig. 1 (b). As $\overline{w}_2^{(4)}$ decreases (i.e., the frequency-selectivity of the channel decreases), we can use less pilot symbols in the frequency direction (i.e., to increase $\hat{y}_2$), and vice versa. The proposed approach can also be applied to the use of other interpolators for channel estimation.

To verify the analytic results, the performance is evaluated in terms of the BER when the proposed pilot pattern is used with linear interpolators. Table 1 summarizes the simulation parameters of the OFDM system and propagation channel [11]. For given channel condition and pilot density, the optimum pilot spacing is analytically determined as $(\hat{x}_1, \hat{y}_2) = (12,6)$. For performance comparison, we also evaluate the performance when $(x_1, y_2) = (8,9)$ and $(18,4)$, which have the same pilot density. It can be seen from Fig. 4 that the use of the optimum pilot pattern provides the

Table 1. Simulation condition.

FFT size	512
Number of subcarriers	512
Subcarrier spacing (Δf)	125 kHz
Symbol duration (T_s)	8us (6.4us +1.6us: guard interval)
Modulation	QPSK
Channel	Rayleigh (Jakes' spectrum)
Multipaths	8 (Uniform, 50 ns equi-spaced)
Carrier frequency	5.8 GHz
Normalized Doppler frequency ($f_d T_s$)	0.02455
Pilot density (D)	1/72 (1.4 %)

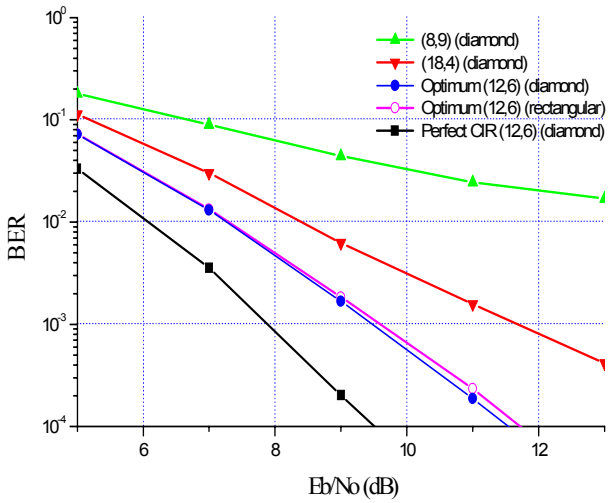

Fig. 4. BER Performance due to pilot pattern when *D*=1/72.

BER performance significantly better than the use of non-optimum ones. It can also be seen that the use of diamond pilot pattern is slightly better than the use of rectangular one.

IV. CONCLUSIONS

In this paper, for a given pilot density, we have analytically determined the optimum pilot pattern for channel estimation of the OFDM systems with the use of conventional interpolators. The use of a diamond shape provides estimation performance slightly better than the use of any other shape. The optimum spacing of the pilot symbol depends upon the pilot density, the Doppler spectrum and the power delay profile. The analytic result is verified by computer simulation.

RERFERENCE

[1] Y. Li, "Pilot-symbol-aided channel estimation for OFDM in wireless systems," *IEEE Trans. Veh. Tech.*, vol. 49, pp. 1207-1215, July 2000.

[2] S. Coleri, M. Ergen, A. Puri and A. Bahai, "Channel estimation techniques based on pilot arrangement in OFDM systems," *IEEE Trans. Broadcasting*, vol. 48, pp. 223-229, Sept. 2002.

[3] K. F. Lee and D. B. Williams, "Pilot-symbol-assisted channel estimation for space-time coded OFDM systems," *EURASIP J. Applied Signal Process.*, vol. 5, pp. 507-516, May 2002.

[4] F. Said and H. Aghvami, "Linear two dimensional pilot assisted channel estimation for OFDM systems," *IEE Conf. Telecommun.'98*, pp. 32-36, Apr. 1998.

[5] M. J. F. -G. Garcia, S. Zazo and J. M. Paez-Borrallo, "Pilot patterns for channel estimation in OFDM," *Electronics Letters*, vol. 36, pp. 1049-1050, June 2000.

[6] F. Tufvesson and T. Maseng, "Pilot assisted channel estimation for OFDM in mobile cellular systems," *Proc. VTC'97*, pp. 1639-1643, May 1997.

[7] P. Hoeher, S. Kaiser and P. Robertson, "Two-dimensional pilot-symbol-aided channel estimation by Wiener filtering," *Proc. ICASSP'97*, pp. 1845-1848, Apr. 1997.

[8] R. Nilsson, O. Edfors, M. Sandell and P. O. Borjesson, "An analysis of two-dimensional pilot-symbol assisted modulation for OFDM," *Proc. ICPWC'97*, pp. 71-74, Dec. 1997.

[9] A. V. Oppenheim and R. W. Schafer, *Discrete-time signal processing*, second edition, Prentice Hall, 1999.

[10] D. E. Dudgeon and R. M. Mersereau, *Multidimensional Digital Signal Processing*, Prentice Hall, 1984.

[11] N. Maeda, H. Atarashi, S. Abeta and M. Sawahashi, "Throughput comparison between VSF-OFCDM and OFDM considering effect of sectorization in forward link broadband packet wireless access," *Proc. VTC'02 Fall*, pp. 47-51, Sept. 2002.